Correlation of temperature induced conformation change with optimum catalytic activity in the recombinant G/11 xylanase A from *Bacillus subtilis* strain 168 (1A1)

Mário T. Murakami[a], Raghuvir K. Arni *,[a], Davi S. Vieira[c], Léo Degrève *,[c], Roberto Ruller[b], Richard J. Ward[c,*]

[a] *Department of Physics, IBILCE/UNESP, Cristovão Colombo 2265, São José do Rio Preto, São Paulo, Brazil*
[b] *Department of Cellular and Molecular Biology, FMRP, Universidade de São Paulo, Avenida Bandeirantes 3900, Ribeirão Preto, São Paulo, Brazil*
[c] *Department of Chemistry, FFCLRP, Universidade de São Paulo, Avenida Bandeirantes 3900, Ribeirão Preto, São Paulo, Brazil*

Received 9 September 2005; revised 30 September 2005; accepted 19 October 2005

Available online 2 November 2005

Edited by Miguel De la Rosa

Abstract The 1.7 Å resolution crystal structure of recombinant family G/11 β-1,4-xylanase (rXynA) from *Bacillus subtilis* 1A1 shows a jellyroll fold in which two curved β-sheets form the active-site and substrate-binding cleft. The onset of thermal denaturation of rXynA occurs at 328 K, in excellent agreement with the optimum catalytic temperature. Molecular dynamics simulations at temperatures of 298–328 K demonstrate that below the optimum temperature the thumb loop and palm domain adopt a closed conformation. However, at 328 K these two domains separate facilitating substrate access to the active-site pocket, thereby accounting for the optimum catalytic temperature of the rXynA.
© 2005 Federation of European Biochemical Societies. Published by Elsevier B.V. All rights reserved.

Keywords: Thermostable enzyme; Crystal structure; Molecular dynamics

1. Introduction

Xylan is the most abundant hemicellulose in plant cell walls, and is comprised of a β-(1,4)-D-xylopyranoside backbone which is generally substituted by acetyl, arabinose and 4-*O*-methyl-glucuronose residues. A wide variety of microorganisms produce xylan-degrading enzymes, and the enzymatic cleavage of β-1,4-xylosidic linkages is performed by β-1,4-xylan xylanohydrolase (EC 3.2.1.8). Xylanases have been grouped into families F/10 and G/11 on the basis of amino acid sequence homology, hydrophobic cluster and three-dimensional structural analysis [1]. The structures of the family G/11 xylanases contain an α-helix and two twisted β-sheets forming a jellyroll fold [2,3], yet despite the high similarity of amino acid sequences and structural homology, the G/11 xylanases exhibit a wide range of temperature optima of catalytic activity.

A common approach to address the question as to the structural basis of thermostability uses the comparison between the crystal structures of mesophilic and thermophilic homologues. Superposition of the crystal structures of thermostable xylanases from *Thermoanaerobacterium saccharoclyticum* [4] and *Clostridium thermocellum* [5] reveals that an N-terminal extension forms an additional β-strand that increases the number of hydrogen bonds in the β-sandwich finger domain, and has led to the suggestion that the N-terminal regions of these enzymes contribute to their thermostability. Hydrophobic interactions and salt bridges have also been suggested to be important structural features for thermostability [6,7]. The hydrophobic core of G/11 xylanases extends along the entire length of the internal surface of the β-sandwich and is rich in highly conserved tyrosine and tryptophan residues, and indeed the thermostability of family G/11 xylanases has been improved through the introduction of aromatic interactions by site-directed mutagenesis [7]. Salt bridges are distributed over the whole surface of the protein, and mutagenesis of His149 (located on the opposite side of the active site) to Phe or Gln did not modify the catalytic activity, but significantly improved the thermal stability [8]. Furthermore, the thermostability of family G/11 xylanases has been improved by the inclusion of additional surface charges [9], arginine residues [10] and disulphide bonds [11,12].

Several experimental approaches have been used to improve the thermostability and thermophilicity of xylanases including chemical modification, cross-linking, immobilization, treatment with additives and protein engineering [13], and the results of these studies suggest that multiple factors may contribute to the structural basis of thermostability. In an effort to identify the structural basis of thermostability, we have focused on understanding the structural changes in the G/11 xylanases at various temperatures leading up to the optimum temperature for catalysis. With the aim of identifying and delineating the structural basis for the catalytic activity at elevated temperature of these industrially relevant enzymes, we report the crystal structure at 1.7 Å resolution and molecular dynamics studies in the range of temperature of a recombinant thermophilic family G/11 xylanase from *Bacillus subtilis* 1A1 (rXynA).

2. Materials and methods

2.1. Expression, purification, crystallization and data collection

The gene encoding XynA was expressed in *Escherichia coli* strain DH5α and the recovered protein was purified as described previously [14]. The expression system yields 26 mg L^{-1} of culture of

*Corresponding authors. Fax: +55 0 16 36338151.
E-mail address: rjward@fmrp.usp.br (R.J. Ward).

Abbreviations: rXynA, recombinant family G/11 β-1,4-xylan xylanohydrolase from *Bacillus subtilis* strain 1A1; RMSD, root mean square deviation

0014-5793/$30.00 © 2005 Federation of European Biochemical Societies. Published by Elsevier B.V. All rights reserved.
doi:10.1016/j.febslet.2005.10.039

protein (7.7% total yield), and N-terminal sequencing and mass-spectrometry have confirmed that the signal peptide has been correctly processed to give as the final product the expected 185 amino acid protein [14]. Crystals suitable for X-ray diffraction experiments were obtained from 2 μL droplets containing 2.8 mg mL^{-1} of protein, 1.2 M sodium tartrate and 1% dioxane [15]. The data were collected to 1.7 Å using synchrotron radiation and a MARCCD detector at the CPr beam line, LNLS (Laboratorio Nacional de Luz Sincrotron, Campinas, Brazil). Intensity data were integrated, scaled and reduced to obtain structure factor amplitudes with the HKL package [16].

2.2. Structure solution and refinement

The crystal structure of the rXynA was solved by molecular replacement techniques with the AMoRe package [17] using the atomic coordinates of the G/11 xylanase from *Bacillus circulans* (PDB code 1XNB, [18]) as the search model. Positional and individual isotropic thermal factor refinements were carried out using REFMAC5 [19] as incorporated in the CCP4 suite (Collaborative Computational Project Number 4, 1994). The $2F_{ob} - F_c$ and $F_{ob} - F_c$ electron density maps were examined and the protein model was manually adjusted after each refinement cycle using the TURBO FRODO program [20]. The stereochemistry of the final model was analyzed using PROCHECK [21]. The atomic coordinates and structure factors of XynA have been deposited with the Protein Data Bank (code: 1XXN).

2.3. Thermal denaturation monitored by circular dichroism

Thermal denaturation experiments were performed using a J-810 spectropolarimeter equipped with a Peltier-type temperature controller (PTC423S-JASCO Inc., Tokyo, Japan) with a heating rate of 1 °C min^{-1} using 1 cm path-length cuvettes and a protein concentration of 100 μg mL^{-1} in 20 mM phosphate buffer at pH 6.0. The change in the ellipticity signal at 216 nm was monitored over the temperature range of 25–75 °C (298–348 K). The fitting of the thermal denaturation curve assumed a two-state mechanism and used a least squares fitting routine derived from the van't Hoff equation as described previously [22,23].

2.4. Sequence alignment and structural analysis

The alignment of 5 amino acid sequences from the corresponding 3D structures was performed by structure-based alignment utilizing the 3D-coffee alignment tool [24]. The superpositioning and structural analysis was performed by TURBO FRODO program [20] and the ConSurf program was used for the identification of functional regions by surface-mapping using phylogenetic data [25].

2.5. Molecular dynamics simulations

Molecular dynamics calculations were performed as isothermal–isobaric ensemble under physiological conditions at temperatures of 298, 308, 318 and 328 K. All molecular dynamics simulations were run with the GROMACS 3.2 software package [26] using the GROMOS-96 (43a1) force field [27]. The temperature and pressure were controlled using the Berendsen method [28] with coupling time constants of 0.1 and 3.0 ps for temperature and pressure, respectively. The LINCS algorithm [29] was used to constrain protein covalent bonds involving hydrogen atoms, and the SETTLE algorithm [30] was used to constrain water molecules. The "leap-frog" algorithm [31] was used to integrate the equations of motion with a time step of 2.0 fs over a total time of 5.0 ns. Initial velocities were obtained from a Maxwell distribution at 298 K, and long-range interactions were treated using the particle-mesh Ewald sum (PME) method [32] with a cutoff of 1.5 nm. The long-range electrostatic contributions were updated every 20 fs, and the van der Waals interactions were calculated with a cutoff of 1.5 nm. The edges of the cubic simulation boxes were initially fixed at 8.5 nm, and contained about 19000 simple-point charge (SPC) water molecules [33] (concentration of ~53.0 mol L^{-1}). The Cl^- and Na^+ counter-ions were inserted in the most electrostatically favorable positions in order to locally neutralize the system. All simulations were equilibrated for 100 ps restraining the positions of the protein atoms. The atomic trajectories were analyzed by monitoring the peptide and residue root mean square deviation (RMSDs) of atomic positions relative to the crystal structure.

3. Results and discussion

3.1. Crystal structure

Crystals of rXynA were obtained as previously described [15], and belong to the orthorhombic space group $P2_12_12$ with cell parameters a = 50.90, b = 70.37 and c = 42.04 Å. The Matthews coefficient (V_m = 1.68 Å^3 Da^{-1}) indicates the presence of one molecule per asymmetric unit with a corresponding solvent content of 26.15%. Table 1 presents the full refinement statistics of the final model, which shows that rigid-body model refinement using data in the resolution range of 20.0–2.5 Å resulted in a correlation coefficient of 65.4% and a R_{factor} of 36.4%. Structure refinement converged to a crystallographic residual of 16.2% for all data between 42.03 and 1.75 Å (without sigma or intensity cutoff, R_{free} = 20.9% for 5% of the data). The refined structural model of the rXynA contains 185 amino acid residues, 1 tartrate molecule, and 112 solvent water molecules per asymmetric unit. Stereochemical analysis of the final model indicates that the main-chain dihedral angles for all residues are located in the permitted regions of the Ramachandran diagram, and that the RMSD from ideal values are within permitted ranges. Residual electron density was observed at the surface of the molecule, and was attributed to a single tartrate molecule which is hydrogen bonded by Thr106, Gln135, Ser136, and two solvent water molecules, and forms additional hydrogen bonds with the Ser74 in a symmetry equivalent protein molecule.

Fig. 1A shows that the rXynA has the canonical β-sandwich 'right-hand' fold of family G/11 xylanases, in which the individual β-strands thread back and forth between the two packed β-sheets to form the finger and palm domains. Resi-

Table 1
Data collection and refinement statistics

Data collection	
Temperature (K)	100
Wavelength used (Å)	1.427
Detector	MARCCD
Space group	P2(1)2(1)2
Unit cell parameters (Å)	a = 50.90, b = 70.37 and c = 42.04
Resolution range (Å)	42.03–1.70
No. of observed reflections	21487
Data completeness (%)	83.5 (81.3)
No. of unique reflections	14449
I/sigma(I)	7.16 (2.5)
[a]R_{merge} (%)	9.2 (26.9)
V_M (Å^3 Da^{-1})	1.68
Solvent content (%)	26.15
Molecules per asymmetric unit	1
Molecular replacement	
Correlation coefficients (%)	
Rotation	33.7
Translation	52.3
Rigid body refinement	65.4
Rigid body refinement R-factor (%)	36.4
Refinement	
R_{factor} (%)	16.2
R_{free} (%)	20.9
RMSD bond distances (Å)	0.01
RMSD bond angles (°)	1.42
Average B_{factor} (Å^2)	23.1

Values in parentheses are for the high-resolution bin.
[a]$R_{merge} = \Sigma|I(h)_I - \{I(h)\}|/\Sigma\{I(h)\}$, where I_h is the observed intensity of the ith measurement of reflection h and $\{I(h)\}$ is the mean intensity of reflection h calculated after scaling.

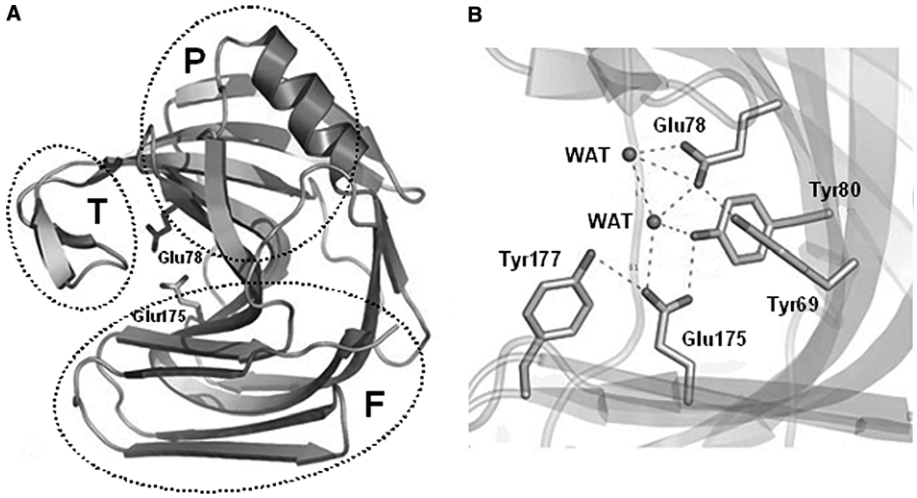

Fig. 1. The three-dimensional structure of the rXynA. (A) Ribbon representation including the catalytic residues Glu78 and Glu 172 located at the base of the cleft formed by the palm (P) and fingers (F) domains. Access to the active site cleft is determined by the position of the thumb (T) domain. (B) Detail of the active site region showing the network of hydrogen bonds formed by Tyr69, Glu78, Tyr80, Glu175, Tyr177 and the positionally conserved solvent water (WAT) molecules.

dues lining the cleft formed between these two domains contribute to the substrate binding and active sites of the protein. An extended loop between the B7 and B8 strands forms the so-called thumb domain, and a loop between the B6 and B9 strands forms a cord between the two β-sheet domains (Fig. 1A) [34]. The active site is defined by a network of hydrogen bonded residues including Glu78 and Glu175, two structurally conserved water molecules, and the neighboring Tyr69 and Tyr80 residues that are involved in substrate binding (Fig. 1B). A two-step acid–base mechanism for xylan hydrolysis has been proposed in which proton transfer occurs to and from an oxygen atom in an equatorial position at the anomeric center [35]. All the positions of the catalytic residues involved in this mechanism are fully conserved in the rXynA crystal structure.

3.2. Thermostability of the rXynA

Previous studies have shown that the profile of the far ultraviolet circular dichroism spectra shows a minimum at 216 nm [14], which is typical for β-sheet rich proteins and is in accord with the secondary structure content observed in the crystal structure. Fig. 2 presents the thermal denaturation curve of the rXynA as monitored by the loss of secondary structure measured at 216 nm, which reveals that the transition from the native to the denatured enzyme starts at a temperature of 328 K. Previous results have demonstrated that the rXynA has an optimum temperature for catalysis of 55 °C (328 K) [14], which corresponds exactly to the maximum temperature at which the rXynA maintains a native secondary structure. At temperatures above this value both the catalytic activity and β-sheet secondary structure are lost. With the aim of understanding the structural basis of the thermostability of this protein, a series of molecular dynamics simulations were performed at four temperatures between 298 and 328 K.

3.3. Molecular dynamics

The atomic trajectories of rXynA were analyzed by monitoring the RMSD of protein atom positions and the mean RMSD

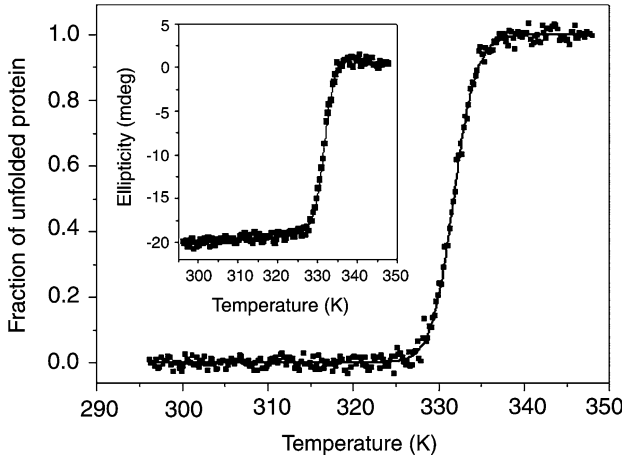

Fig. 2. Thermal denaturation of the rXynA as monitored by the change in circular dichroism in the ultraviolet region between 200 and 250 nm. The fraction of unfolded protein as a function of temperature (main panel). The inset presents the raw ellipticity data at 216 nm measured during the experiment (for clarity only half the total number of data points are presented). In both the main panel and insert, the solid lines represent the curves obtained after data fitting (see Section 2), which yielded a melting temperature (T_m) of 331.8 K.

per residue during a time period of 5 ns during the molecular dynamics calculations in the isothermal–isobaric ensemble under physiological conditions at 298, 308, 318 and 328 K. Fig. 3 shows the RMSD of rXynA at different temperatures, from which mean RMSD values of 0.130 ± 0.016 nm (at 298 K), 0.148 ± 0.015 nm (308 K), 0.143 ± 0.014 nm (318 K) and 0.175 ± 0.030 nm (328 K) were calculated. These results demonstrate that the protein conformations are highly stable at all temperatures used in the simulations, an overview confirmed by the mean RMSD values per residue at the different temperatures (Fig. 4). Mean RMSD values of most positions in the palm domain (residues 41–50, 68–81, 93–110, 126–132 and 145–168), on which are located several active site and aromatic substrate-binding residues, demonstrate low deviations at all temperatures. The majority of positions in the finger do-

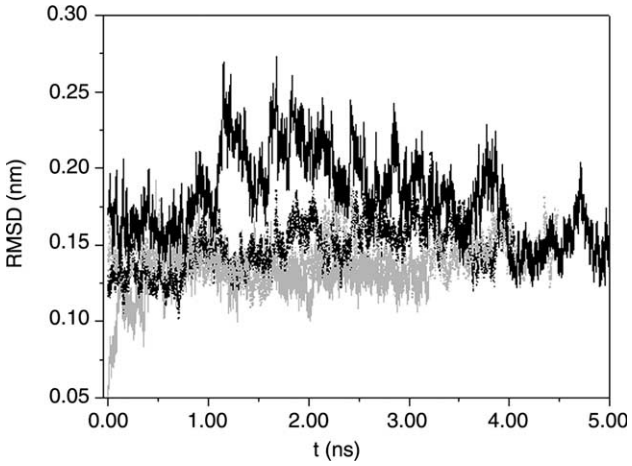

Fig. 3. RMSD of atomic positions in the molecular dynamics simulations of the rXynA at temperatures of 298 K (solid grey lines), 308 K (dotted black lines), 318 K (dotted grey lines) and 328 K (solid black lines). The positions of the protein atoms in the crystallographic structure were used as the reference for the RMSD calculations.

main (residues 1–40, 52–67, 83–87 and 169–185) also show reduced RMSD values, which suggests that the protein has a generally high stability even at 328 K. In contrast, many regions in the vicinity of glycine residues (including positions 10–15, 20–22, 26–28, 100–104, 118–124 and 135–140) show a higher mean RMSD per residue at all temperatures, which reflects the elevated mobility of the protein segments containing these residues.

The comparison of the rXynA amino acid sequence with four other G/11 xylanases (Fig. 5) reveals that many tyrosine (Tyr53, Tyr69, Tyr79, Tyr80, Tyr107, Tyr130 and Tyr169) and tryptophan residues (Trp9, Trp71 and Trp155) are highly conserved. These residues not only play a key role in substrate binding, but also contribute to the hydrophobic interactions that confer rigidity and compactness to the palm domain and active-site pocket. Other hydrophobic residues (Val37, Val82, Pro90, Ile120 and Phe125) are also conserved, and are likely to be important in the stability of the secondary and tertiary structures. Fig. 5 further demonstrates that the majority of glycine residues are also highly conserved, and occupy positions throughout the thumb and finger domains and in the cord/connecting loops of the two packed β-sheets. The flexibility of these glycine residues is generally elevated at all temperatures (see Fig. 4), although the regions around Gly12-Gly14, Gly23, Gly28 and Gly62 show no clear pattern of temperature dependent conformation change. In contrast, the region around Gly122 on the β-turn in the thumb domain presents a clear trend in which an increase in temperature results in significantly increased conformation change.

The thumb domain is highly conserved throughout the family G/11 xylanases, and comparison of crystal structures has suggested that the thumb loop is the most flexible region of the molecule [36]. This is supported by molecular dynamics simulations, and has led to the suggestion that the elevated flexibility of the thumb loop is important to allow substrate access to the active site residues [37]. The distance variations in the molecular dynamics simulations between these two domains are shown in Fig. 6, which reveals that the distance between the palm domain and thumb loop is around of 1.30 nm at temperatures below the catalytic temperature optimum. However, at the optimum catalytic temperature of 328 K, the distance between the palm and thumb domains increases to 1.65 nm, and the substrate-binding cleft adopts an open conformation. These distances are significantly greater than those observed in previous molecular dynamics simulation studies [37], and we speculate that the optimum temperature of catalytic activity is the consequence of the exposure of the active site cleft by temperature dependent conformation change in the thumb domain.

These results are in accord with previous NMR studies which demonstrate that the conformation changes of the xylanase A from *Bacillus circulans* on binding a substrate analogue are confined to the substrate binding region and are relatively slight, the exception being the significant conformation changes observed in the thumb domain [38]. Both the NMR study and the molecular dynamics simulation reported here

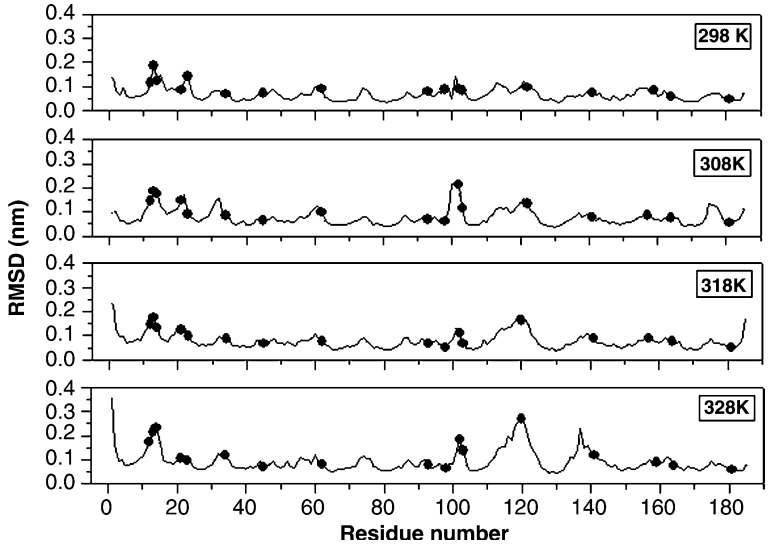

Fig. 4. RMSD per residue. The results of four separate simulations are presented, at temperatures between 298 and 328 K (as indicated on the figure). Conserved glycine residues at positions 12, 13, 14, 21, 23, 34, 45, 62, 93, 98, 104,105, 122, 159, 164 and 181 are indicated by the solid circles.

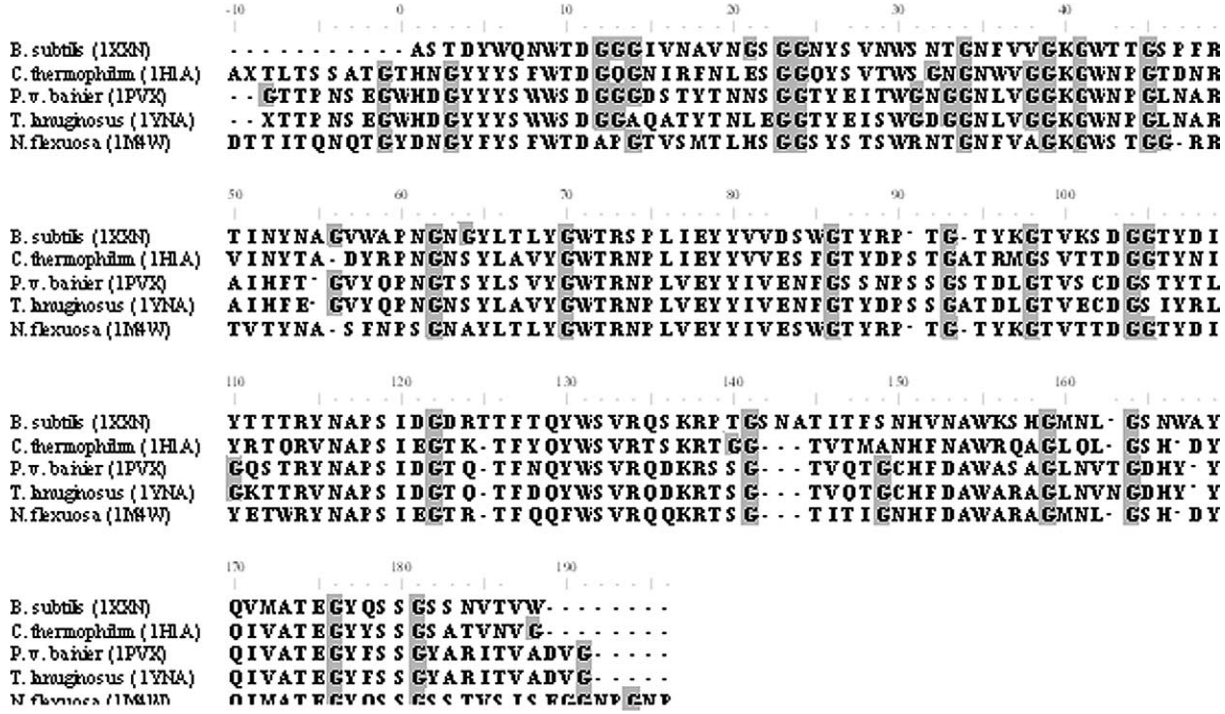

Fig. 5. Multiple amino acid sequence alignment of the rXynA (PDB code 1XXN) with other family G/11 xylanases. The sequences and corresponding PDB codes are; endoxylanase 11A from *Chaetomium thermophilum*, (1H1A, [39]), xylanase from *Paecilomyces varioti bainier* (1PVX, [40]), endo-1,4-β-xylanase from *Thermomyces lanuginosus*, (1YNA, [36]), and endoxylanase from *Nonomuraea flexuosa* (1M4W, [39]). The adopted numbering scheme starts at −10 so as to place the N-terminal alanine residue of rXynA at position 1. Glycine residues are shown with a grey background.

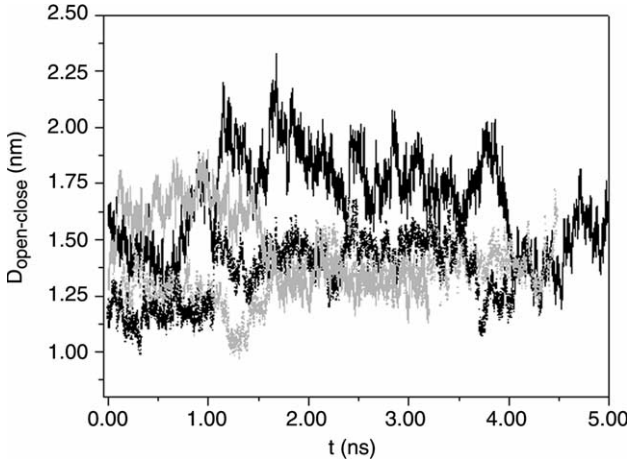

Fig. 6. Variation in the distance between the thumb and palm domains during the molecular dynamics simulations of the rXynA at temperatures of 298 K (solid grey lines), 308 K (dotted black lines), 318 K (dotted grey lines) and 328 K (solid black lines).

indicate that the palm and finger domains are essentially rigid structures, and the enhanced flexibility necessary for catalysis lies in those segments in the immediate vicinity of glycine residues. This conclusion focuses attention on the temperature dependence of the conformation change in the thumb domain, which is identified as a key event in determining the optimum catalytic temperature of the enzyme. This work suggests that site-directed mutagenesis studies with the aim of decreasing the flexibility in this region may offer an alternative strategy for rational design of thermostable xylanases.

Acknowledgements: This work was funded by FAPESP doctorate fellowships 01/08012-0 (R.R.), 03/13082-3 (M.T.M.), 03/01457-2 (DSV), FAPESP SMOLBnet project 01/7537-2, CNPq and the Pro-Reitoria de Pesquisa-USP (PRP-USP).

References

[1] Coutinho, P.M. and Henrissat, B. (1999). Available from: <http://afmb.cnrs-mrs.fr/CAZY/>.
[2] Henrissat, B. and Davies, G. (1997) Structural and sequence-based classification of glycoside hydrolases. Curr. Opin. Struct. Biol. 7, 637–644.
[3] Henrissat, B. and Davies, G.J. (2000) Glycoside hydrolases and glycosyltransferases. Families, modules, and implications for genomics. Plant Physiol. 124, 1515–1519.
[4] Lee, Y.E., Lowe, S.E., Henrissat, B. and Zeikus, J.G. (1993) Characterization of the active site and thermostability regions of endoxylanase from *Thermoanaerobacterium saccharolyticum* B6A-RI. J. Bacteriol. 175, 5890–5898.
[5] Fontes, C.M., Hazlewood, G.P., Morag, E., Hall, J., Hirst, B.H. and Gilbert, H.J. (1995) Evidence for a general role for non-catalytic thermostabilizing domains in xylanases from thermophilic bacteria. Biochem. J. 307 (Pt 1), 151–158.
[6] Eriksson, A.E., Baase, W.A., Zhang, X.J., Heinz, D.W., Blaber, M., Baldwin, E.P. and Matthews, B.W. (1992) Response of a protein structure to cavity-creating mutations and its relation to the hydrophobic effect. Science 255, 178–183.
[7] Georis, J., de Lemos Esteves, F., Lamotte-Brasseur, J., Bougnet, V., Devreese, B., Giannotta, F., Granier, B. and Frere, J.M. (2000) An additional aromatic interaction improves the thermostability and thermophilicity of a mesophilic family 11 xylanase: structural basis and molecular study. Protein Sci. 9, 466–475.
[8] Plesniak, L.A., Connelly, G.P., Wakarchuk, W.W. and McIntosh, L.P. (1996) Characterization of a buried neutral histidine residue in *Bacillus circulans* xylanase: NMR assignments, pH titration, and hydrogen exchange. Protein Sci. 5, 2319–2328.

[9] Torronen, A. and Rouvinen, J. (1997) Structural and functional properties of low molecular weight endo-1,4-beta-xylanases. J. Biotechnol. 57, 137–149.
[10] Turunen, O., Vuorio, M., Fenel, F. and Leisola, M. (2002) Engineering of multiple arginines into the Ser/Thr surface of *Trichoderma reesei* endo-1,4-beta-xylanase II increases the thermotolerance and shifts the pH optimum towards alkaline pH. Protein Eng. 15, 141–145.
[11] Wakarchuk, W.W., Sung, W.L., Campbell, R.L., Cunningham, A., Watson, D.C. and Yaguchi, M. (1994) Thermostabilization of the *Bacillus circulans* xylanase by the introduction of disulfide bonds. Protein Eng. 7, 1379–1386.
[12] Andrews, S.R., Taylor, E.J., Pell, G., Vincent, F., Ducros, V.M., Davies, G.J., Lakey, J.H. and Gilbert, H.J. (2004) The use of forced protein evolution to investigate and improve stability of family 10 xylanases. The production of Ca^{2+}-independent stable xylanases. J. Biol. Chem. 279, 54369–54379.
[13] Gupta, M.N. (1991) Thermostabilization of proteins. Biotechnol. Appl. Biochem. 14, 1–11.
[14] Ruller, R., Rosa, J.C., Faca, V.M., Greene, L.J. and Ward, R.J. (2005). Efficient constitutive expression of *Bacillus subtilis* Xylanase A in *Escherichia coli* DH5alpha under the control of the Bacillus BsXA promotor. Biotechnol. Appl. Biochem., in press.
[15] Murakami, M.T., Ruller, R., Ward, R.J. and Arni, R.K. (2005) Crystallization and preliminary X-ray crystallographic studies of the mesophilic xylanase A from *Bacillus subtilis* 1A1. Acta Cryst. F61, 219–220.
[16] Otwinowski, Z. and Minor, W. (1997) Processing of X-ray diffraction data collected in oscillation mode. Meth. Enzymol. 276, 307–326.
[17] Navaza, J. (1994) AMoRe: an automated package for molecular replacement. Acta Crystallogr. A50, 157–163.
[18] Wakarchuk, W.W., Campbell, R.L., Sung, W.L., Davoodi, J. and Yaguchi, M. (1994) Mutational and crystallographic analyses of the active site residues of the Bacillus circulans xylanase. Protein Sci. 3, 467–475.
[19] Murshudov, G.N., Vagin, A.A. and Dodson, E.J. (1997) Refinement of macromolecular structures by the maximum-likelihood method. Acta Crystallog., 240–255.
[20] Jones, T.A. (1985) Interactive computer graphics: FRODO. Methods Enzymol. 115.
[21] Laskowski, R.A., MacArthur, M.W., Moss, D.S. and Thorton, J.M. (1993) PROCHECK: a program to check the stereochemical quality of protein structure. J. Appl. Crystallogr. 26.
[22] Sa, J.M., Chioato, L., Ferreira, T.L., De Oliveira, A.H., Ruller, R., Rosa, J.C., Greene, L.J. and Ward, R.J. (2004) Topology of the substrate-binding site of a Lys49-phospholipase A2 influences Ca^{2+}-independent membrane-damaging activity. Biochem. J. 382, 191–198.
[23] Yadav, S. and Ahmad, F. (2000) A new method for the determination of stability parameters of proteins from their heat-induced denaturation curves. Anal. Biochem. 283, 207–213.
[24] Poirot, O., Suhre, K., Abergel, C., O'Toole, E. and Notredame, C. (2004) 3DCoffee@igs: a web server for combining sequences and structures into a multiple sequence alignment. Nucleic Acids Res. 32, W37–W40.
[25] Glaser, F., Pupko, T., Paz, I., Bell, R.E., Bechor-Shental, D., Martz, E. and Ben-Tal, N. (2003) ConSurf: identification of functional regions in proteins by surface-mapping of phylogenetic information. Bioinformatics 19, 163–164.
[26] Lindahl, E., Hess, B. and van der Spoel, D. (2001) GROMACS 3.0: A package for molecular simulation and trajectory analysis. J. Mol. Mod. 7, 306–317.
[27] van Gunsteren, W.F., Billeter, S.R., Eising, A.A., Hünenberger, P.H., Krüger, P., Mark, A.E., Scott, W.R.P. and Tironi, I.G. (1996) Biomolecular Simulation: The GROMOS96 Manual and User Guide, Biomos, Groningen.
[28] Berendsen, H.J.C., Postma, J.P.M., DiNola, A. and Haak, J.R. (1984) Molecular dynamics with coupling to an external bath. J. Chem. Phys. 81, 3684–3690.
[29] Hess, B., Becker, H., Berendsen, H.J. and Fraaije, J.G.E.M. (1997) Lincs: a linear constraint solver for molecular simulations. J. Comp. Chem. 18, 1463–1472.
[30] Miyamoto, S. and Kollman, P.A. (1992) SETTLE: An analytical version of the SHAKE and RATTLE algorithm for rigid water models. J. Comp. Chem. 13, 952–962.
[31] Hockney, R.W. and Goel, S.P. (1974) Quiet high-resolution computer models of a plasma. J. Comp. Phys. 14, 148–158.
[32] Darden, T., York, D. and Pedersen, L. (1993) Particle mesh Ewald. An $N\log(N)$ method for Ewald sumsin large systems. J. Chem. Phys. 98, 10089–10092.
[33] Berendsen, H.J.C., Postma, J.P.M., van Gunsteren, W.F. and Hermans, J. (1981) Interactions models for water in relation to protein hydration, in: Intermolecular Forces (Pullman, B., Ed.), Reidel Publishing Company, Dordrecht.
[34] Torronen, A., Harkki, A. and Rouvinen, J. (1994) Three-dimensional structure of endo-1,4-beta-xylanase II from Trichoderma reesei: two conformational states in the active site. Embo J. 13, 2493–2501.
[35] Sinnot, M.L. (1990) Catalytic mechanisms of enzymic glycosyl transfer. Chem. Rev. 90, 1171–1202.
[36] Gruber, K., Klintschar, G., Hayn, M., Schlacher, A., Steiner, W. and Kratky, C. (1998) Thermophilic xylanase from *Thermomyces lanuginosus*: high-resolution X-ray structure and modeling studies. Biochemistry 37, 13475–13485.
[37] Muilu, J., Torronen, A., Perakyla, M. and Rouvinen, J. (1998) Functional conformational changes of endo-1,4-xylanase II from *Trichoderma reesei*: a molecular dynamics study. Proteins 31, 434–444.
[38] Connelly, G.P., Withers, S.G. and McIntosh, L.P. (2000) Analysis of the dynamic properties of *Bacillus circulans* xylanase upon formation of a covalent glycosyl-enzyme intermediate. Protein Sci. 9, 512–524.
[39] Hakulinen, N., Turunen, O., Janis, J., Leisola, M. and Rouvinen, J. (2003) Three-dimensional structures of thermophilic beta-1,4-xylanases from *Chaetomium thermophilum* and *Nonomuraea flexuosa*. Comparison of twelve xylanases in relation to their thermal stability. Eur. J. Biochem. 270, 1399–1412.
[40] Eswaramoorthy, S., Vithayathil, P.J. and Viswamitra, M.A. (1994) Crystallization and preliminary X-ray crystallographic studies of thermostable xylanase crystals isolated from *Paecilomyces varioti*. J. Mol. Biol. 243, 806–808.